Improving the Airborne Remote Sensing of Soil Moisture: Estimating Soil Effective Temperature

Paul M. O'Neill[1,2], Remy Dehaan[1,3], Jeffrey P. Walker[4], and Iain Hume[1,5]

Final Report, 18 April 2008

Abstract

Obtaining measurements of the near-surface soil water content from passive microwave observations requires knowledge of the soil effective temperature, which is a function of the soil temperature and moisture profiles. Detailed information on these profiles is not available from airborne remote sensing, but the effective temperature can be estimated via thermal infrared observations of the land surface. Current estimation techniques were developed for bare soil only, and do not account for the effects of vegetation. We have performed a simulation study which investigates the influences of vegetation and intra-day soil temperature and moisture variations. We find that, unless vegetation is taken into account, the so-called 'C parametrisation' performs poorly for leaf area index values $\gtrsim$3. We introduce a technique that models the intra-day variations in the ratio between the effective and surface temperatures. This technique performs particularly well if a term for the near-surface soil moisture is included and vegetation information in available.

1 Introduction

The near-surface soil moisture is an important parameter in hydrological, meteorological and agricultural applications. In agriculture, for example, the near-surface soil moisture affects seed germination and the breakdown of organic material. Moreover, measurements of the near-surface water content can be assimilated into models that predict *root-zone* soil moisture (e.g., Das et al., 2008, and references therein).

The thermal radiation emitted by the soil surface peaks at a wavelength of $\sim$10 μm. This radiation may also be observed at microwave wavelengths with an intensity that depends on the soil temperature and emissivity. The emissivity is related to the near-surface water content such that the presence of water reduces the microwave brightness. Passive microwave observations, airborne and satellite, can thus be used to measure directly the water content (e.g., Ulaby et al., 1986, see Section 2).

[1]E H Graham Centre for Agricultural Innovation (NSW Department of Primary Industries and Charles Sturt University).

[2]School of Computing & Mathematics, Charles Sturt University, Locked Bag 588, Wagga Wagga NSW 2678.

[3]School of Environmental Sciences, Charles Sturt University, Locked Bag 588, Wagga Wagga NSW 2678.

[4]Department of Civil and Environmental Engineering, The University of Melbourne, Melbourne.

[5]Wagga Wagga Agricultural Institute, NSW Department of Primary Industries, Private Mail Bag, Pine Gully Road, Wagga Wagga, New South Wales, 2650.

Obtaining measurements of the near-surface soil water content from passive microwave observations requires an estimation of the soil effective temperature ($T_{\rm EFF}$). The effective temperature is a function of the soil temperature and moisture *profiles*. The moisture profile is important because the range of soil depths that influence $T_{\rm EFF}$ will increase as the soil water content decreases.

It is not possible to directly measure entire temperature and moisture profiles using airborne or satellite instruments. However, thermal infrared (TIR) observations may be performed simultaneously with microwave observations, yielding a composite canopy/soil-skin temperature ($T_{\rm TIR}$). The relationship between $T_{\rm EFF}$ and $T_{\rm TIR}$ has previously been studied for the case of bare soil, allowing one to estimate $T_{\rm EFF}$ (e.g., Choudhury et al., 1982; Wigneron et al., 2001, 2008). The effects of near-surface soil moisture and soil texture have been studied, but the impact of vegetation has not yet been included in these models.

For some agricultural studies it is necessary to understand the influence of vegetation on estimating $T_{\rm EFF}$. For example, an airborne platform performing microwave and thermal infrared measurements could monitor variations in the soil moisture profile over a growing season. This, of course, will involve observing vegetated land cover.

The relationship between the soil effective temperature and soil-skin temperature has been studied previously using temperature and moisture profiles observed during a dry down period (e.g., Choudhury et al., 1982). In the absence of observations, a dry down can be simulated. Wigneron et al. (2008) very recently used simulations to investigate the influence of soil properties on effective temperature. We have followed a similar approach and have used profiles generated by a mechanistic heat and water transfer model to investigate both the influences of vegetation on deriving $T_{\rm EFF}$ from $T_{\rm TIR}$, and the impact of intra-day soil temperature and moisture variations.

2 Theory

In this Section we present briefly certain aspects of the theory that underpins passive microwave measurements of soil moisture. The microwave emission from soil has been modelled using both coherent and noncoherent models (see Schmugge and Choudhury, 1981, and references therein). We are concerned here only with a noncoherent model that relies on an estimation of soil effective temperature.

In the '*zero-order*' (or '*Fresnel*') model (Schmugge and Choudhury, 1981; Ulaby et al., 1986), the observed microwave brightness temperature, $T_{\rm B}$, depends on the soil emissivity, e, and the effective temperature according to the equation

$$T_{\rm B} = e \ T_{\rm EFF} \tag{1}$$

The emissivity is calculated using the well-known Fresnel equations, which describe the reflection and transmission of electromagnetic radiation at an interface between materials having different values of dielectic constant. In the zero-order model, the interface between the soil and air is considered. In general, e depends on polarisation and the radiometer look-angle. For a nadir look-angle, e is identical for horizontal and vertical polarisations, and is given by

$$e = 1 - \left| \frac{\sqrt{\varepsilon} - 1}{\sqrt{\varepsilon} + 1} \right|^2 \tag{2}$$

where ε is the complex dielectric constant of the near-surface soil layer.

The dielectric constant of moist soil can be modelled as a function of the volumetric water content, θ, and soil textural properties (e.g., Wang and Schmugge, 1980). For observations at 1.4 GHz (L-band), the emissivity depends on the average θ in the $\sim$0–2.5 cm range (Wang, 1987; Raju et al., 1995), with the exact moisture sampling depth depending on the shape of the moisture profile.

The effective temperature is related to the temperature and moisture profiles according to the following expression (Choudhury et al., 1982)

$$T_{\mathrm{EFF}} = \int_0^\infty T_{\mathrm{S}}(z)\ \alpha(z)\ \exp\left[-\int_o^x \alpha(z')\ dz'\right]\ dz \tag{3}$$

where T_{S} and α are, respectively, the soil thermodynamic temperature and attenuation coefficient at depth z.

The attenuation coefficient is a function of the real, ε', and imaginary, ε'', components of the dielectric constant, and depends also on the microwave wavelength, λ, as

$$\alpha(z) = \frac{4\pi}{\lambda}\varepsilon''(z)/2(\varepsilon'(z))^{1/2} \tag{4}$$

It is via Eqn. 4 that the effective temperature depends on the moisture profile. For a very moist soil, the thermal emission from deep layers is absorbed in the overlying soil. In this case, the temperature of those deep layers does not contribute much to the calculation of T_{EFF}. For a very dry soil, however, the absoption of the microwave radiation is reduced, so the thermal emission from deep layers can reach the soil surface.

The presence of vegetation is likely to have three impacts on relating T_{EFF} with a composite canopy/soil-skin temperature. First, the canopy shades the underlying soil, thereby reducing the soil heat flux. This effect has been seen in observations of a maize crop in which the canopy temperature exceeded the soil skin temperature (Hornbuckle and England, 2005). Second, in addition to shading, a transpiring canopy will transfer latent heat to the atmosphere. One might then expect the canopy temperature to be *lower* than that of the soil skin. In this case, a thermal infrared observation would underestimate the temperature of the soil skin. Lastly, the extraction of water from the root-zone will markedly affect the shape of the soil moisture profile.

3 Simulations

We used the Simultaneous Heat and Water model (SHAW; e.g., Flerchinger et al., 1998) to generate a series of soil temperature and moisture profiles. SHAW simulates the flow of heat, water and solutes though a one-dimensional soil-vegetation-atmosphere system. Up to fifty soil nodes, with corresponding properties (e.g., texture, hydraulic properties), can be defined. A multi-layer canopy with a number of different plant species, including residue, can also be defined.

The SHAW model requires the input of atmospheric forcing data. Two meteorological stations were operating during the National[1] Airborne Field Experiment in November 2006 (Walker et al., 2006). We used observations from the CSIRO station to obtain forcing data for a typical clear sky day during that campaign. The net radiation, air temperature, humidity and wind speed of the forcing data can be seen in Fig. 1. The same data were used for all days in the simulations.

[1] http://www.nafe.unimelb.edu.au

Each simulation uses a series of 40 days, with 1 hour time steps. A constant rate of precipitation is simulated during the first 10 days, which saturates the soil profile. The last 30 days then comprise the dry down period. The day time (0700 to 1800 hrs) profiles from the last 30 days are used in our study.

In determining the surface energy balance, SHAW calculates the longwave radiation flux emerging from the soil-vegetation system. This calculation provides a composite canopy/soil-skin thermal infrared temperature. The exact soil effective temperature for each pair of temperature and moisture profiles was determined using Eqns. 3 and 4. A nadir look-angle and microwave frequency of 1.4 GHz was assumed for all simulations.

Twenty-six soil nodes were defined, from the surface down to a depth of 4 m. In all simulations we used a silty clay loam soil, which matches field data used by Chanzy et al. (1997) and Wigneron et al. (2001) to investigate effective temperature. The soil properties were set to be identical for all nodes, and a single generic plant species was used. We performed simulations for bare soil and ten values of leaf area index (LAI) in the range 0.5–5, with the vegetation dry mass being set to 0.2×LAI kg m^{-2}. A list of soil and vegetation properties used in running the SHAW model is presented in Table 1.

4 Results

4.1 Profiles and general relationships

In Fig. 2 we present representative profiles of soil temperature and volumetric water content. Profiles are shown for bare soil simulations and those using a leaf area index of 2.5. Fig. 2 highlights that, for a given set of forcing data, the shape of the temperature and moisture profiles will depend on the vegetation coverage. The impact of water extraction by roots is clearly seen down to the rooting depth of 50 cm. For the case of bare soil, the soil-skin water content at 1300 hrs is at its minimum value ($\sim$0.05 cm^3 cm^{-3}) by day 5. For the vegetated profiles, the water content is low but does not reach its minimum value until day 30. The soil-skin temperature, T_0, exhibits a similar effect. For bare soil, the surface temperature at 1300 hrs does not increase by more than 2 K between days 5 and 30. For the vegetated simulations, however, there is an increase of 16 K over the same time period. It is interesting to note also that the maximum surface temperature for the vegetated profiles is 9 K greater than that for bare soil, despite the effects of shading.

In Fig. 3 we present the difference between the composite canopy/soil-skin temperature (T_{TIR}) and the temperature (T_0) of the soil skin only. The difference at a time of 1300 hrs is plotted as a function of the day number of the dry down period, and is shown for LAIs of 0.5, 1.0, 2.5, and 5.0. These plots show that our simulations comprise a range of profiles. Some profiles are dominated by canopy shading, while most simulated values of T_{TIR} reveal the cooling effects of transpiration, particularly so as the dry down progresses. We should expect, therefore, that the relationship between T_{EFF} and T_{TIR} will change as the soil dries, even if the relationship between T_{EFF} and T_0 were not vary.

In Fig. 4, we plot the relationship between effective temperature and soil skin temperature for the case of bare soil. As seen in previous work, there exists a clear relationship between these two variables. This relationship varies as a function of both the hour of day and the number days since the start of the dry down period. Fig. 5 shows the relationship between effective temperature and composite canopy/soil-skin temperature for representative values of LAI. It is clear that the range of T_{EFF}, and its relationship with T_{TIR}, depends on LAI.

4.2 Model 1: the C parametrisation

The effective temperature has previously been modelled as a function of the soil skin temperature, deep soil temperature (T_∞) and a coefficient (C) using the following expression (Choudhury et al., 1982).

$$T_{\rm EFF} = T_\infty + (T_0 - T_\infty)\, C \tag{5}$$

We shall refer to this parametrisation as Model 1.

Model 1 was fitted to the simulated data obtained for bare soil and ten different values of LAI. The deepest soil node in our simulations is at 400 cm, and we used the temperature at this depth, T_{400}, in the place of T_∞. For the vegetated simulations, we used $T_{\rm TIR}$ instead of T_0. The best-fitting values of C as a function of LAI are presented in Fig. 6. The value of C decreases from approximately 0.4 to 0.1 as LAI increases from 0 to 5. Note, however, that the smallest non-zero value of LAI (viz., 0.5) yielded a small increase in C compared to the bare soil value.

To quantify the effectiveness of using the above equation for estimating $T_{\rm EFF}$, we have calculated approximate values of $T_{\rm EFF}$ using the best-fitting values of C. We shall denote such estimates of effective temperatue as $T_{\rm EFF,model}$. We also estimated $T_{\rm EFF}$ for different values of LAI using the bare-soil C value of 0.365. The root-mean-square (RMS) error, bias and standard deviation of the residuals associated with the estimates are presented in Fig. 6. A positive bias corresponds to an overestimate when compared to the exact value given by Eqn. 3, which we shall denote as $T_{\rm EFF,exact}$. It is clear that an improvement may be gained through the application of a vegetation-specific coefficient for LAI values $\gtrsim$1. The magnitude of the bias increases nearly monotonically with LAI, suggesting that the above parametrisation itself may not be appropriate for moderate to high levels of vegetation.

We have also calculated the percentage error associated with estimating $T_{\rm EFF}$ from the best-fitting values of C. The percentage errors are plotted in Fig. 7, as a function of hour of day, for three days during the dry down period. The intra- and inter-day variations seen in Fig. 7 qualitatively resemble those presented by Choudhury et al. (1982). We investigate these variations in more detail in Section 4.3.

4.3 Intra- and inter-day variations

As seen in Fig. 4, the relationship between $T_{\rm EFF}$ and T_0 clearly varies over the course of a day and also as the dry down progresses. Theses variations are owing to changes in the soil moisture and temperature profiles. As described in Section 2, the effective temperature depends directly on the moisture profile. Wigneron et al. (2001) accounted for this by expressing C as a function of the 0–3 cm volumetric water content, θ_{0-3}. Diurnal variations in the slope of the temperature profile itself might also be expected to influence the relationship between $T_{\rm EFF}$ and T_0, producing a dependence on hour of day (e.g., Maggioni et al., 2006)

We shall first investigate variations in C. We calculated the value of C for each profile in the *bare soil* simulation. From a total of 360 profiles, 40 profiles have values less than zero, 313 have values in the range 0–1, and 7 have values greater than 1.

Fig. 8 shows the changes in soil temperature (T_0, T_3, T_{400} and $T_{\rm EFF}$), θ_{0-3} and C at 0700 hrs over the duration of the dry down period. Fig. 9 shows variations in the same quantities between 0700 and 1800 hrs on day 15. Fig. 8 exhibits a general trend of decreasing C with θ_{0-3}. This trend, however, is reversed when considering variations over the course of a single day. In this case, the skin temperature decreases after $\sim$1400 hrs, while the temperatures of the deeper

layers, and, therefore, also $T_{\rm EFF}$, continue to increase. This variation in the temperature profile produces an apparent *increase* in C as θ_{0-3} decreases during the day.

The intra- and inter-day variations in C can be seen also in Fig. 10, where we present the mean value of C as a function of hour. The mean C from all profiles is shown, as are the means for days 1–15 and 16–30 of the dry down period. The intra-day variation shows a general increasing trend after 0800 hrs, similar to that seen in the plot for day 15 (see Fig. 9). The inter-day variations depend on hour of day. At 0700 and 1000 hrs, the value of C decreases between the first and second halves of the dry down. At other hours, however, C is higher in the second half of the simulation.

We next calculated the ratio between $T_{\rm EFF}$ and T_0, which we denote as ρ, for all bare soil profiles. In Fig. 11 we plot ρ as a function of hour. The mean ρ from all profiles is shown, as are the means for the first and second halves of the dry down period. The intra-day variations are smooth, with ρ decreasing to a minimum at approximately midday. Clear inter-day variations are seen, which also depend on hour. In the early morning and late afternoon, the mean value of ρ in the second half of the dry down period is either lower than, or very close to, that for the first half. At around midday, however, the mean ρ during the second half is clearly lower.

Finally, in Fig. 12, we present C and ρ as a function of θ_{0-3}. The intra-day variations in C and ρ are dominant. Clear relationships between C and ρ, and θ_{0-3} and ρ, are seen when considering a certain hour in isolation. These relationships depend on time of day. For example, a positive relationship exists between C and θ_{0-3} at 0700 hrs (as was seen in Fig. 8). But this is the only hour for which such a relationship is seen.

4.4 Models 2 and 3: a variable $T_{\rm EFF}$ / $T_{\rm TIR}$ ratio

It is clear from Figs. 10 and 11 that the intra- and inter-day variations are described more simply though ρ rather than C. Therefore, we have explored models in which the effective and composite canopy/soil-skin temperatures are related according to the following expression

$$T_{\rm EFF} = \rho \ T_{\rm TIR} \tag{6}$$

We first consider the coefficient ρ to be a function only of hour of day. In this model, which we refer to as Model 2, ρ is expressed as

$$\rho = 1 \ - \ (1 - \rho_{\rm min}) \sin\left(\frac{\pi}{12}\left[H - H_0\right]\right) \tag{7}$$

where H is the hour of day. The parameter $\rho_{\rm min}$ is the minimum value of ρ, which occurs at close to midday, and H_0 is the hour at which ρ equals unity, which is early in the morning.

Model 2 was fitted to the bare soil and vegetated simulations, and the results are presented in Fig. 13. The model parameters do not change much with an increase in LAI above 1. The quality of the fit is best for bare soil and for relatively high values of LAI. Note that, for most values of LAI, the mean $T_{\rm EFF,model}$ is lower than $T_{\rm EFF,exact}$ (i.e., negative bias). Despite the difference between the bare soil and vegetated parameter values, the performance of Model 2 is relatively insensitive to the use of parameter values found for bare soil.

We next considered a dependence on the 0–3 cm volumetric water content. In this model, which we refer to as Model 3, ρ is defined as follows

$$\rho = \rho_{\rm zero} \ \left(\frac{\theta_{0-3}}{\theta_{\rm zero}}\right)^{\gamma} \tag{8}$$

where $\rho_{\rm zero}$ and $\theta_{\rm zero}$ both depend on the hour of day. The dependence of $\rho_{\rm zero}$ on hour of day is given simply by the sinusoidal expression for ρ shown in Eqn. 7.

A time dependence for the parameter $\theta_{\rm zero}$ is required to account for the reduction in θ_{0-3} between 0700 and 1800 hrs (see Fig. 9). The hourly variation of $\theta_{\rm zero}$ can be described approximately as

$$\theta_{\rm zero} = a_0 + a_1 H \tag{9}$$

As seen in Fig. 12, the relationship between ρ and θ_{0-3} (at a given hour) varies over the course of a day. In Model 3, the shape of this relationship is determined by the index γ in Eqn. 8. This parameter depends approximately sinusoidally on hour and can, therefore, be related to $\rho_{\rm zero}$ as

$$\gamma = b_0 + b_1 \rho_{\rm zero} \tag{10}$$

In summary, Model 3 estimates $T_{\rm EFF}$ as a function of $T_{\rm TIR}$, H and θ_{0-3}, with six parameters, viz., $\rho_{\rm min}$, H_0, a_0, a_1, b_0 and b_1. The values of these six parameters depend on leaf area index.

We fitted Model 3 to the simulated profiles and the results are presented in Figs. 14 and 15. The best-fitting parameter values all exhibit a general trend, either increasing or decreasing, as LAI varies in the range 0.5–5. For all parameters, with the exception of H_0, the bare soil results do not follow this trend. The model performs very well when using vegetation-specific parameter values. The RMS error is $<$1 K and the bias is negligible for all values of LAI. However, Model 3 performs poorly when applying the bare soil parameters to the vegetation simulations.

A visual impression of the ability of Models 1, 2 and 3 to estimate $T_{\rm EFF}$ can be seen in Fig. 16, where we plot $T_{\rm EFF,exact}$ versus $T_{\rm EFF,model}$. In addition to showing the results for bare soil, we present those for LAI values of 0.5 and 2.5, which are representative of the LAI range 0.5–5. Model 3 clearly performs best, although at the expense of being the most complex model. Note especially the improvement in using Model 3 for an LAI of 0.5.

5 Discussion

We have conducted a simulation study to investigate the influence of vegetation, and intra-day soil temperature and moisture variations, on the relationship between soil effective temperature and a composite canopy/soil-skin temperature. The SHAW model was used to simulate a number of dry down periods, each lasting 30 days. Simulations were conducted for 11 values of leaf area index in the range 0–5. The relationship between $T_{\rm EFF}$ and $T_{\rm TIR}$ was modelled using day time (0700–1800 hrs) profiles. We applied the C parametrisation (Model 1) and also introduced two new models (Models 2 and 3), which describe the variation in the $T_{\rm EFF}$/$T_{\rm TIR}$ ratio, ρ, as a function of hour and the 0–3 cm volumetric water content. We discuss below our results and comment on possible future work.

5.1 Intra-day variations

An increase in the near-surface volumetric water content is expected to produce an increase in C. This moisture-dependence is very clearly seen in the field data of (Holmes et al., 2006). Wigneron et al. (2001) introduced a moisture term into the C parametrisation, and their form of

the model is used in the algorithm developed for the Soil Moisture and Ocean Salinity mission (Wigneron et al., 2007).

In contrast, our simulations of a 30 day dry down period show a dominance of intra-day variations in C. These variations are owing to the phase and amplitude differences between T_{TIR} and the temperatures of soil layers contributing to T_{EFF}. Note, however, that a relationship between C and θ_{0-3} *is* apparent when considering a single hour in isolation.

Intra-day variations have been seen previously. de Rosnay et al. (2006), working with two years of field data, found that diurnal effects in the estimation of T_{EFF} were pronounced for a very dry and warm period (see their fig. 4.43). During this period, the C parametrisation over-estimated T_{EFF} in the afternoon (i.e., the model C was too high). The maximum discrepancy occured early in the afternoon, after which the estimated T_{EFF} became closer to the actual T_{EFF}. The reduction in the discrepancy during the afternoon was presumably owing to an increase in the *actual* value of C, just as we have see in our simulations.

Intra-day variations in C are likely to be minimised though using a near-surface temperature instead of T_{TIR}. Indeed, in previous studies a near-surface temperature (e.g., T_5) has been used instead of the soil skin temperature (Wigneron et al., 2001; Holmes et al., 2006; de Rosnay et al., 2006). This was found to yield better estimates than using a skin temperature. In the work of de Rosnay et al. (2006, see their figs. 4.42 and 4.43), the parametrisation developed by Holmes et al. (2006) performed well in modelling the diurnal variations in effective temperature. This is, in part, owing to the use of T_5, which was seen to vary roughly in phase with T_{EFF}. The choice of depth for the deep soil temperature (T_∞) in the C parametrisation is also likely to affect the results. de Rosnay et al. (2006) used T_{50}, whereas we have used T_{400} (see additional comments in Section 5.4). The intra-day variations in C, however, are primarily owing to our use of T_{TIR} instead of, e.g., T_5.

The only temperature that can be measured directly with airborne TIR observations is the composite vegetation canopy/soil-skin temperature. It is useful, then, to account for intra-day variations in estimating T_{EFF}. These variations are more easily described with the T_{EFF}/T_{TIR} ratio than with C. We introduced a new model in which ρ varies as a function of hour of day. Moreover, we include a term for the 0–3 cm volumetric water content, which is able to account for *inter*-day variations.

5.2 Model Comparison

In Fig. 17 we show again the RMS errors associated with estimating T_{EFF} using Models 1,2 and 3. We refer to this figure in comparing the performances of these models.

We first consider the scenario in which T_{EFF} is estimated using the best-fitting parameter values found for each value of LAI (Fig. 17 top). Model 3 performs better that Models 1 and 2 for all values of LAI. Comparing now just Models 1 and 2, which do not include a moisture term, we see that Model 1 is better (i.e., a lower RMS error) over the LAI range $\sim$0.5–3. For bare soil or LAI$\gtrsim$3, Model 2 is preferred.

It is useful also to compare the performance of each model when the best-fitting parameters for bare soil are used (Fig. 17 bottom). Model 3 performs well for LAI $\lesssim$0.5, but is otherwise inferior to Models 1 and 2. As before, we can compare just Models 1 and 2 with each other. Model 2 is not as sensitive to the presence of vegetation for LAI$\gtrsim$3, while Model 1 performs better for LAI$\lesssim$3.

In summary, Model 3 is preferred provided that it has been properly calibrated and that vegetation information is available. If, however, the bare soil parameters only are available,

then Model 3 should only be used under conditions of low vegetation. When using a bare soil calibration, Model 1 is preferred over Model 2 for moderate vegetation converage.

5.3 Future directions

It is important now to conduct field observations to establish empirically the imapct of vegetation on estimating T_{EFF}. This can be accomplished though an analysis of the data collected during the National Airborne Field Experiment (NAFE) in 2006 (Walker et al., 2006).

NAFE 2006 was as international campaign coordinated by the University of Melbourne (UMelb). Airborne Research Australia (ARA), in conjunction UMelb, operates a national facility that is capable of conducting passive microwave and thermal infrared observations. The passive L-band microwave radiometer measures the brightness temperature at 1.4 GHz. The spatial resolution of each of its six beams depends on flying height, with the highest resolution being $\sim$50 m. The infrared camera resolution at the same altitude is $\sim$1 m. This facililty was used to collect data near Yanco, New South Wales, during a one-month period. Ground truth data were also collected, such as near-surface soil moisture, vegetation properties, soil roughness and soil temperature.

The NAFE ground truth and airborne data could be used to investigate the relationship between T_{EFF} and T_{TIR}. The soil moisture data can be used to determine the soil emissivity and thereby permit the derivation of T_{EFF} from the airborne measurements of T_{B} (see Eqn. 1). Note that the microwave emissivity depends also on soil roughness, and it is necessary to account for this effect (Ulaby et al., 1986). Vegetation also has an impact on T_{B} in that plants will absorb microwaves from the soil and emit their own. Established techniques exist for modelling the imact of vegetation (e.g., Jackson et al., 2004, and references therein). Fortunately, these techniques utilise similar ground truth and satellite data that would be used to generate spatial data on vegetation LAI. The effective temperature data could then be related to the simultaneous airborne observations of T_{TIR}.

The calibration of models relating T_{EFF} and T_{TIR} will be influenced by the distribution of soil and temperature profiles used in the calibration procedure. For this reason, empirical models should be calibrated using ground truth collected over the time period for which they are to be applied, and for similar soil properties and meteorological conditions.

5.4 Selection of T_{∞}

We used T_{400} as the deep soil temperature in the C parametrisation (Model 1). Previous work has typically used the temperature at a shallower depth. de Rosnay et al. (2006), for example, used T_{50}. In our simulations, T_{400} varied by less than 0.5 K over the duration of the dry down period, and so it can be well approximated with a constant. In comparison, T_{50} increased by $\sim$6 K and exhibited small diurnal variations.

This choice of T_{∞} will certainly affect the results obtained from applying the C parametrisation. Future work should, therefore, investigate the impact of using different depths for T_{∞}. In an operational setting, T_{∞} must itself be derived, with a corresponding level of uncertainty. The uncertainty should be taken into account when assessing the performance of T_{EFF} estimations.

Finally, we note again that the strength of *diurnal* variations in C will primarily be influenced by the choice of the shallower temperature. This is restricted to being T_{TIR} for airborne observations.

References

Chanzy, A., Raju, S., Wigneron, J.-P., 1997. Estimation of soil microwave effective temperature at l and c bands. IEEE Trans. Geosci. Remote Sens. 35, 570–580.

Choudhury, B. J., Schmugge, T. J., Mo, T., 1982. A parameterization of effective soil temperature for microwave emission. J. Geophys. Res. 87 No. C2, 1301–1304.

Das, N. N., Mohanty, B. P., Cosh, M. H., Jackson, T. J., 2008. Modeling and assimilation of root zone soil moisture using remote sensing observations in walnut gulch watershed during smex04. Remote Sens. Environ. 112, 415–429.

de Rosnay, P., Wigneron, J.-P., Holmes, T., Calvert, J.-C., 2006. Parametrisations of the effective temperature for l-band radiometry. inter-comparison and long term validation with smosrex field experiment. In: Mätzler, C., Rosenkranz, P. W., Battaglia, A., Wigneron, J.-P. (Eds.), Thermal Microwave Radiation: Applications for Remote Sensing. IET Electromagnetic Waves Series 52. The Institution of Engineering and Technology, London, United Kingdom, pp. 312–324.

Flerchinger, G. N., Kustas, W. P., Weltz, M. A., 1998. Simulating surface energy fluxes and radiometric surface temperatures for two arid vegetation communities using the shaw model. J. Appl. Meteor. 37, 449–460.

Holmes, T. R. H., de Rosnay, P., de Jeu, R., Wigneron, J.-P., Kerr, Y., Calvert, J.-C., Escorihuela, M. J., Saleh, K., Lemaître, F., 2006. A new parameterization of the effective temperature for l bands radiometry. Geophys. Res. Lett. 33, L07405, doi:10.1029/2006GL025724.

Hornbuckle, B. K., England, A. W., 2005. Diurnal variation of vertical temperature gradients within a field of maize: Implications for satellite microwave radiometry. IEEE Geosci. Remote Sens. Let. 2, 74–77.

Jackson, T. J., Chen, D., Cosh, M., Li, F., Anderson, M., Walthall, C., Doriaswami, P., Hunt, E. R., 2004. Vegetation water content mapping using landsat data derived normalized difference water index for corn and soybeans. Remote Sens. Environ. 92, 475–482.

Maggioni, V., Panciera, R., Walker, J. P., Rinaldi, M., Paruscio, V., Kalma, J. D., Kim, E., 2006. A multi-sensor approach from high resolution airborne soil moisture mapping. In: 30th hydrology and water resources symposium [CD-ROM]. The Institute of Engineers Australia, Launceston, Australia, 4–8 December 2006.

Raju, S., Chanzy, A., Wigneron, J.-P., Calvert, J.-C., Kerr, Y., Laguerre, L., 1995. Soil moisture and temperature profile effects on microwave emission at low frequencies. Remote Sens. Environ. 54, 85–97.

Schmugge, T. J., Choudhury, B. J., 1981. A comparison of radiative transfer models for predicting the microwave emission from soils. Radio Sci. 16, 927–938.

Ulaby, F. T., Moore, R. K., Fung, A. K., 1986. Microwave Remote Sensing, Active and Passive. Volume III: From Theory to Applications. Artech House, Norwood.

Walker, J., Merlin, O., Panciera, R., Kalma, J., Kim, E., Hacker, J., 2006. National airborne field experiments for soil moisture remote sensing. In: 30th hydrology and water resources symposium [CD-ROM]. The Institute of Engineers Australia, Launceston, Australia, 4–8 December 2006.

Wang, J. R., 1987. Microwave emission from smooth bare fields and soil moisture sampling depth. IEEE Trans. Geosci. Remote Sens. GE-25, 616–622.

Wang, J. R., Schmugge, T. J., 1980. An empirical model for the complex dielectric constant of soils as a function of water content. IEEE Trans. Geosci. Electron. GE-18, 288–295.

Wigneron, J.-P., Chanzy, A., de Rosnay, P., Rüdinger, C., Calvert, J.-C., 2008. Estimating the effective soil temperature at l-band as a function of soil properties. IEEE Trans. Geosci. Remote Sens. 46, 797–807.

Wigneron, J.-P., Kerr, Y., Waldteufel, P., Saleh, K., Escorihuela, M.-J., Richaume, P., Ferrazzoli, P., de Rosnay, P., Gurney, R., Calvert, J.-C., Grant, J. P., Guglielmetti, M., Hornbuckle, B., Mätzler, C., Pellarin, T., Schwank, M., 2007. L-band microwave emission of the biosphere (l-meb) model: Description and calibration against exprimental data sets over crop fields. Remote Sens. Environ. 107, 639–655.

Wigneron, J.-P., Laguerre, L., Kerr, Y. H., 2001. A simple parameterization of the l-band microwave emission from rough agricultural soils. IEEE Trans. Geosci. Remote Sens. 39, 1697–1707.

Table 1: Soil and vegetation parameters used in the SHAW simulations.

Soil Properties		Vegetation Properties	
Node depths (cm)	0, 0.5, 1.0, 1.5, 2.0 2.5, 3.0, 3.5, 4.0, 4.5 5.0, 6.0 7.0, 8.0, 9.0 10, 20, 30, 40, 50, 60 70, 80, 90, 100, 400	Leaf orientation	Random
		Albedo	0.15
		Unstressed stomatal resistance (s m^{-1})	100
Percentage sand	11		
Percentage silt	62	Stomatal resistance exponent	5
Percentage clay	27		
Bulk density (kg m^{-3})	1420	Critical leaf water potential (m)	-200
Saturated volumetric water content	0.44		
		Leaf resistance (m^3 s kg^{-1})	1×10^5
Campbell's pore size distribution index	5.5	Root resistance (m^3 s kg^{-1})	2×10^5
		Plant height (m)	0.5
Air-entry potential (m)	-0.2		
		Leaf width (cm)	3
Saturated conductivity (cm h^{-1})	0.439		
		Rooting depth (m)	0.5
Dry soil albedo	0.2		
Soil albedo exponent	1.0		

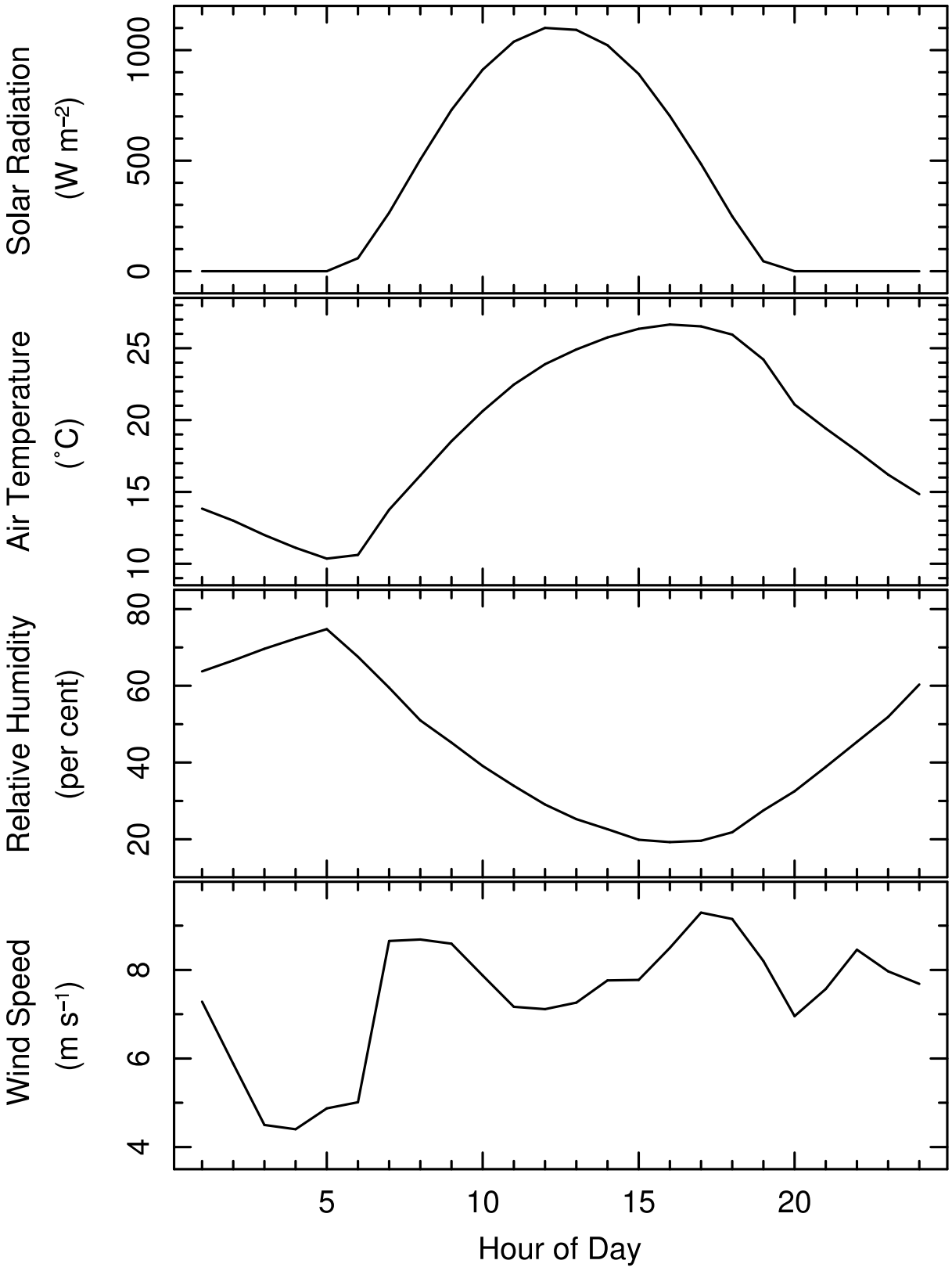

Figure 1: Meterological forcing data used in the SHAW simulations. The solar radiation is that measured on a horizontal surface.

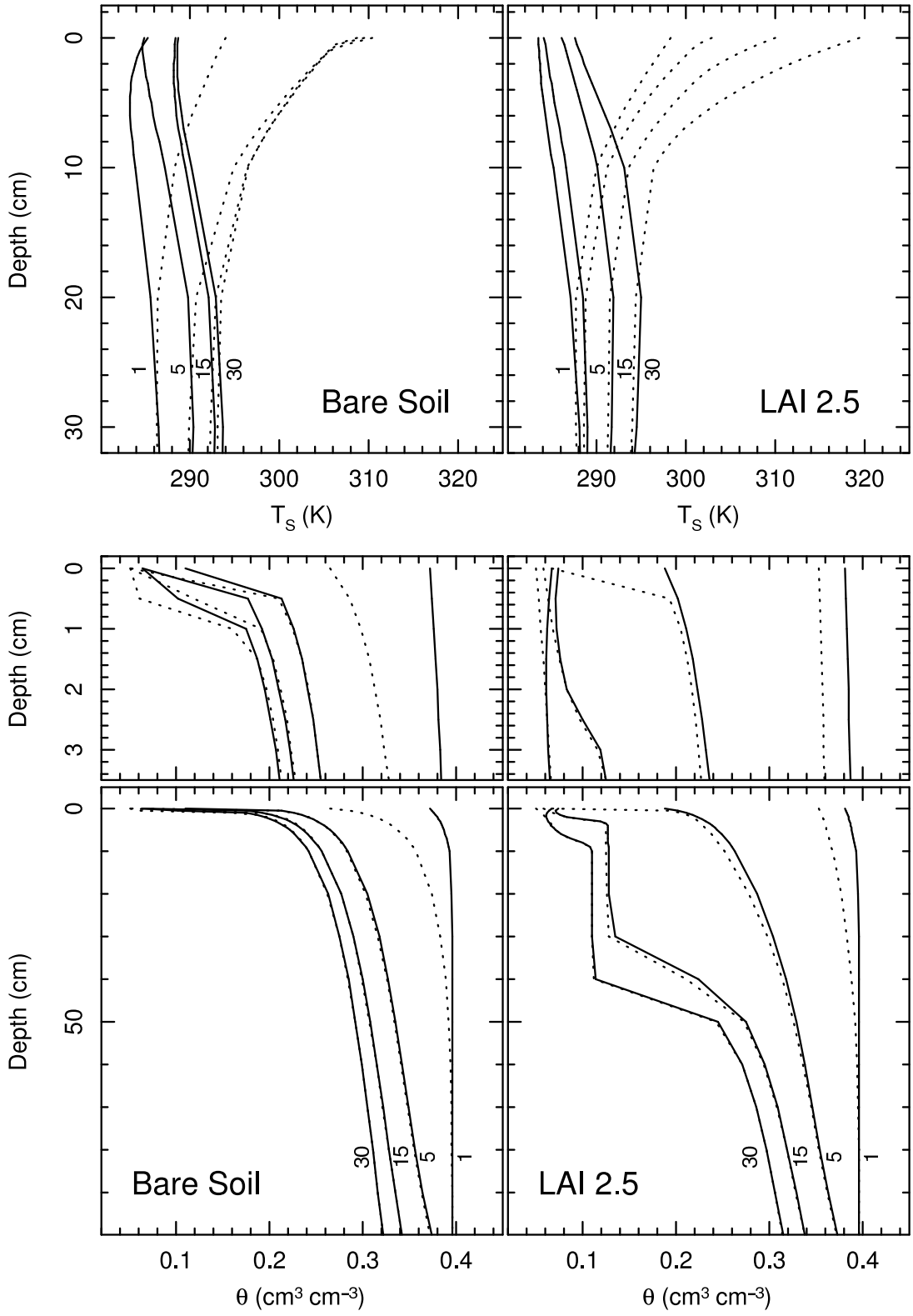

Figure 2: Representative profiles of soil temperature (T_{S}; top panels) and volumetric water content (θ; bottom panels). The day number of the dry down period is shown adjacent to the corresponding profile. The solid and dotted lines represent profiles at 0700 and 1300 hrs, respectively. The water content in the top 3 cm of the profile is shown in the smaller panels. The left- and right-hand panels, respectively, correspond to simulations for bare soil and a leaf area index of 2.5.

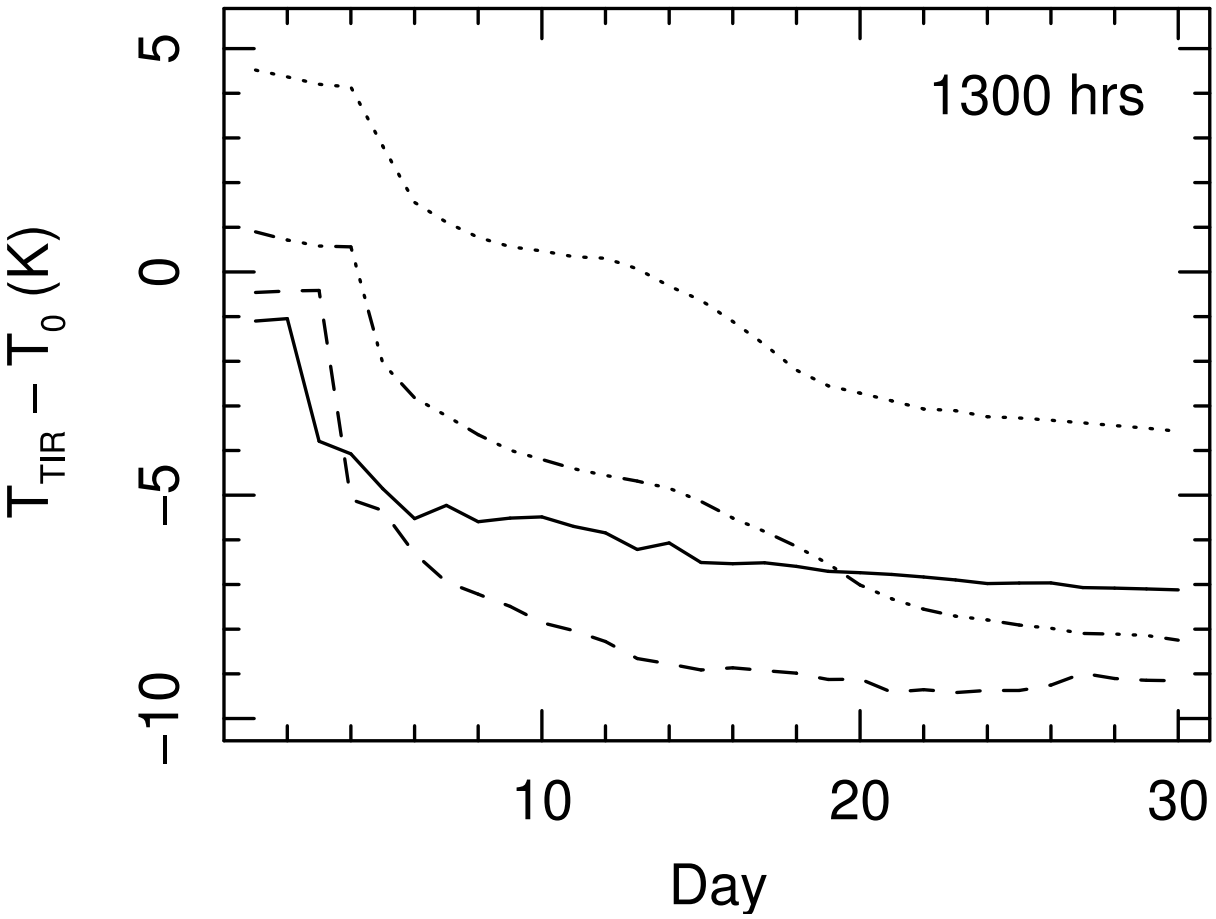

Figure 3: The difference between composite canopy/soil-skin temperature (T_{TIR}) and soil skin temperature (T_0) at 1300 hrs over the duration of the dry down period. The lines correspond to LAIs of 0.5 (solid line), 1.0 (dashed), 2.5 (dotted-dashed), and 5.0 (dotted).

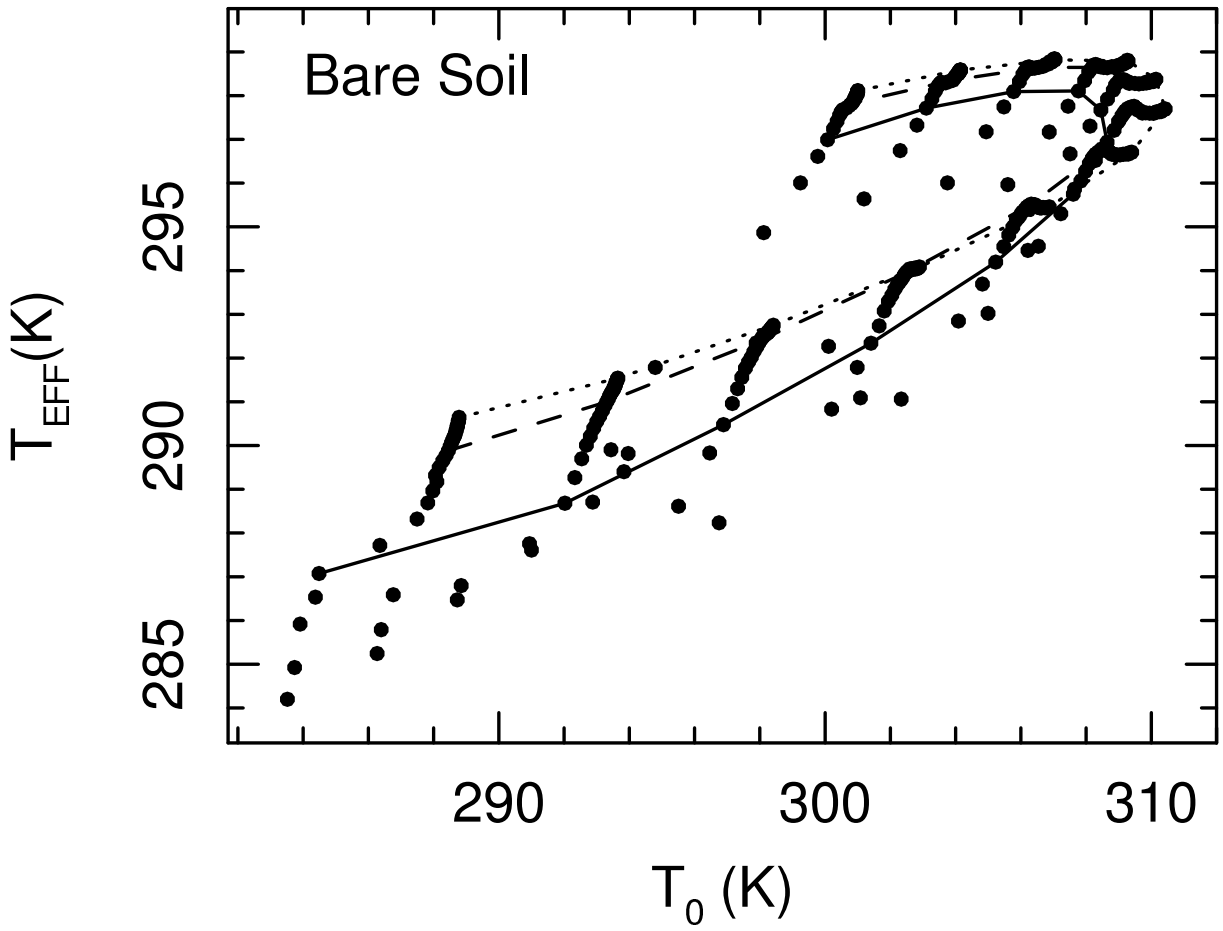

Figure 4: Soil effective temperature (T_{EFF}) versus soil skin temperature (T_0) for bare soil. The lines correspond to day numbers 5 (solid line), 15 (dashed) and 30 (dotted) of the dry down period. The variation in temperature from 0700 to 1800 hrs is seen as a progression along the lines, starting at the bottom-left of the figure.

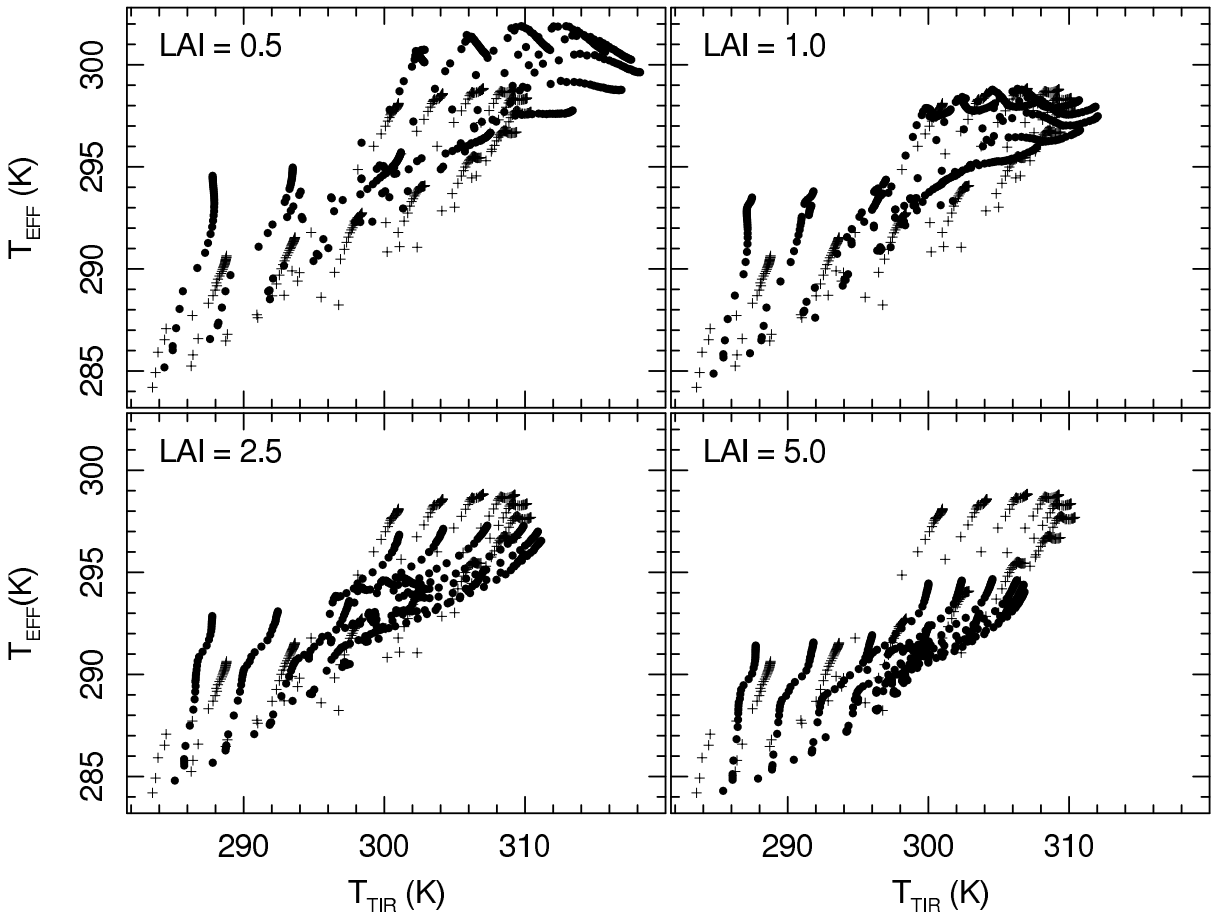

Figure 5: Soil effective temperature ($T_{\rm EFF}$) versus composite canopy/soil-skin temperature ($T_{\rm TIR}$) for LAIs of 0.5, 1.0, 2.5, and 5.0. The solid circles and crosses in each panel correspond to the relevant LAI and bare soil, respectively.

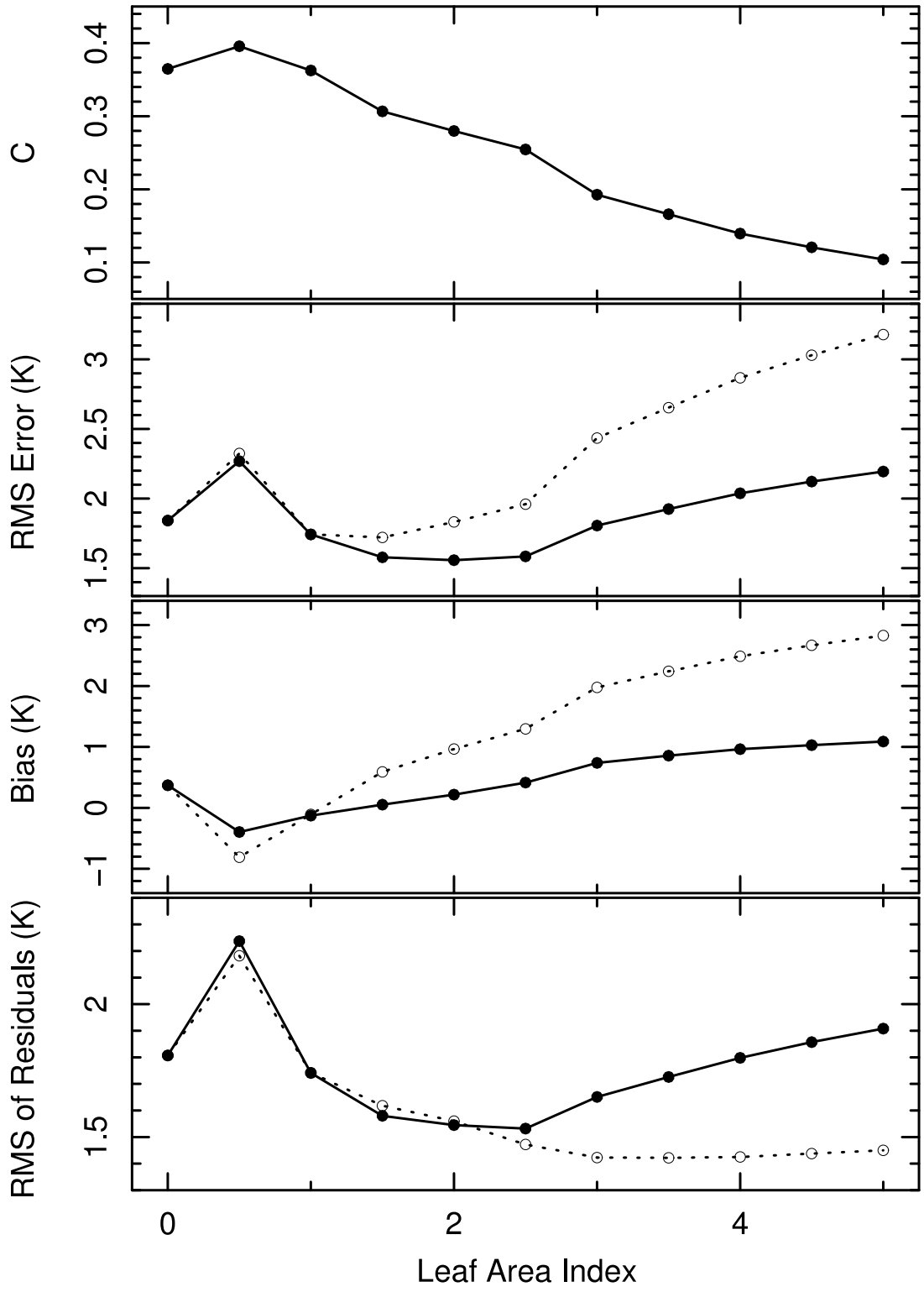

Figure 6: Results from applying the C parametrisation to the simulated profiles. The top panel shows the best-fitting value of C versus leaf area index. The three lower panels, from top to bottom, show the root-mean-square error, bias and standard deviation of the residuals associated with estimating T_{EFF} as a function of T_{TIR} and T_{400}. The solid lines in these panels correspond to estimations using the best-fitting values of C. The dotted lines correspond to estimations using the bare soil value of $C = 0.365$.

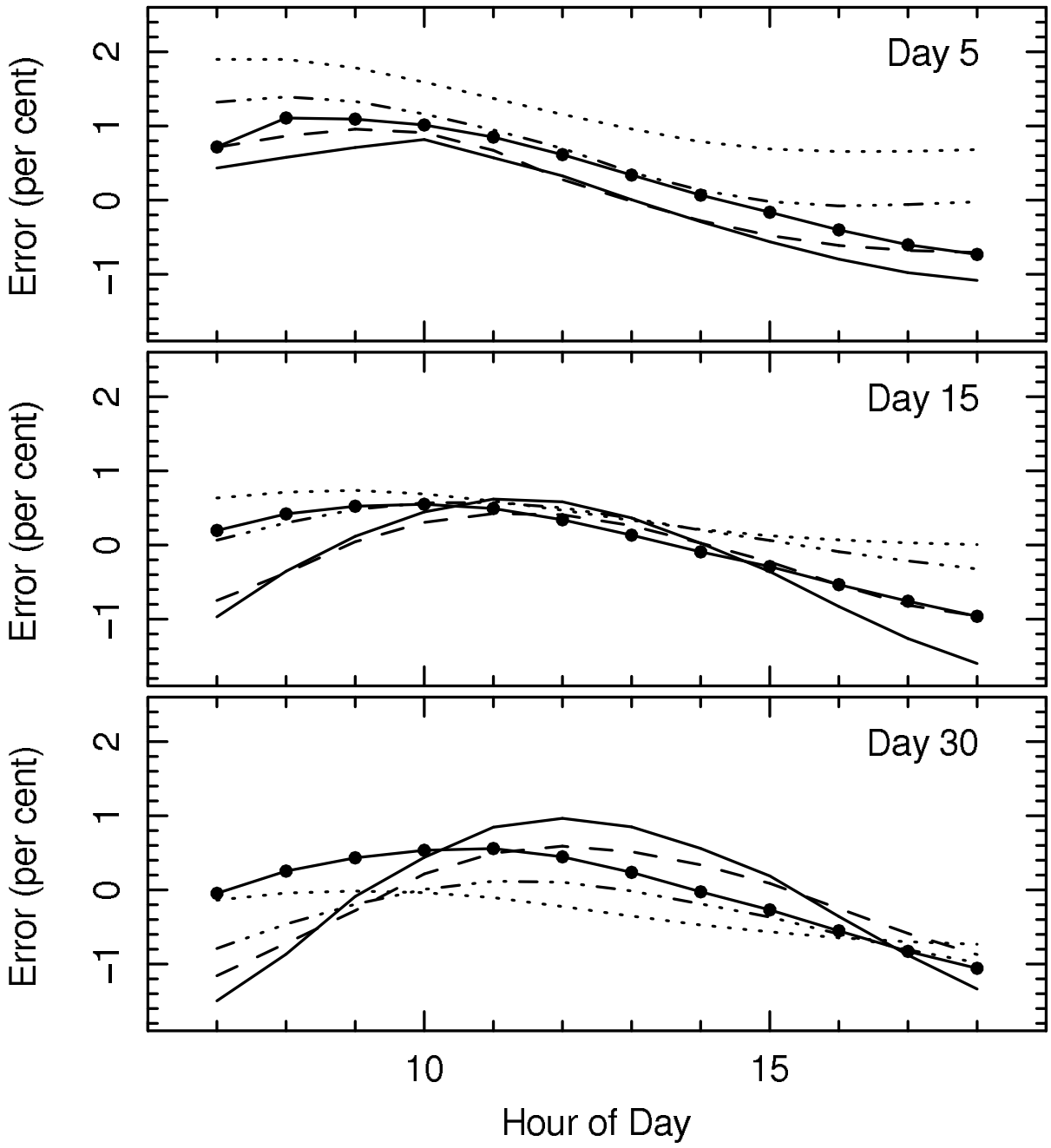

Figure 7: Percentage error associated with estimating T_{EFF} using the best-fitting value of C for each value of LAI. The error is plotted as a function of hour of day for days 5 (top panel), 15 (middle panel) and 30 (bottom panel) of the dry down period. The solid circles indicate the bare soil simulation. The lines without markers correspond to LAIs of 0.5 (solid line), 1.0 (dashed), 2.5 (dotted-dashed), and 5.0 (dotted). A positive error corresponds to an overestimate of T_{EFF}.

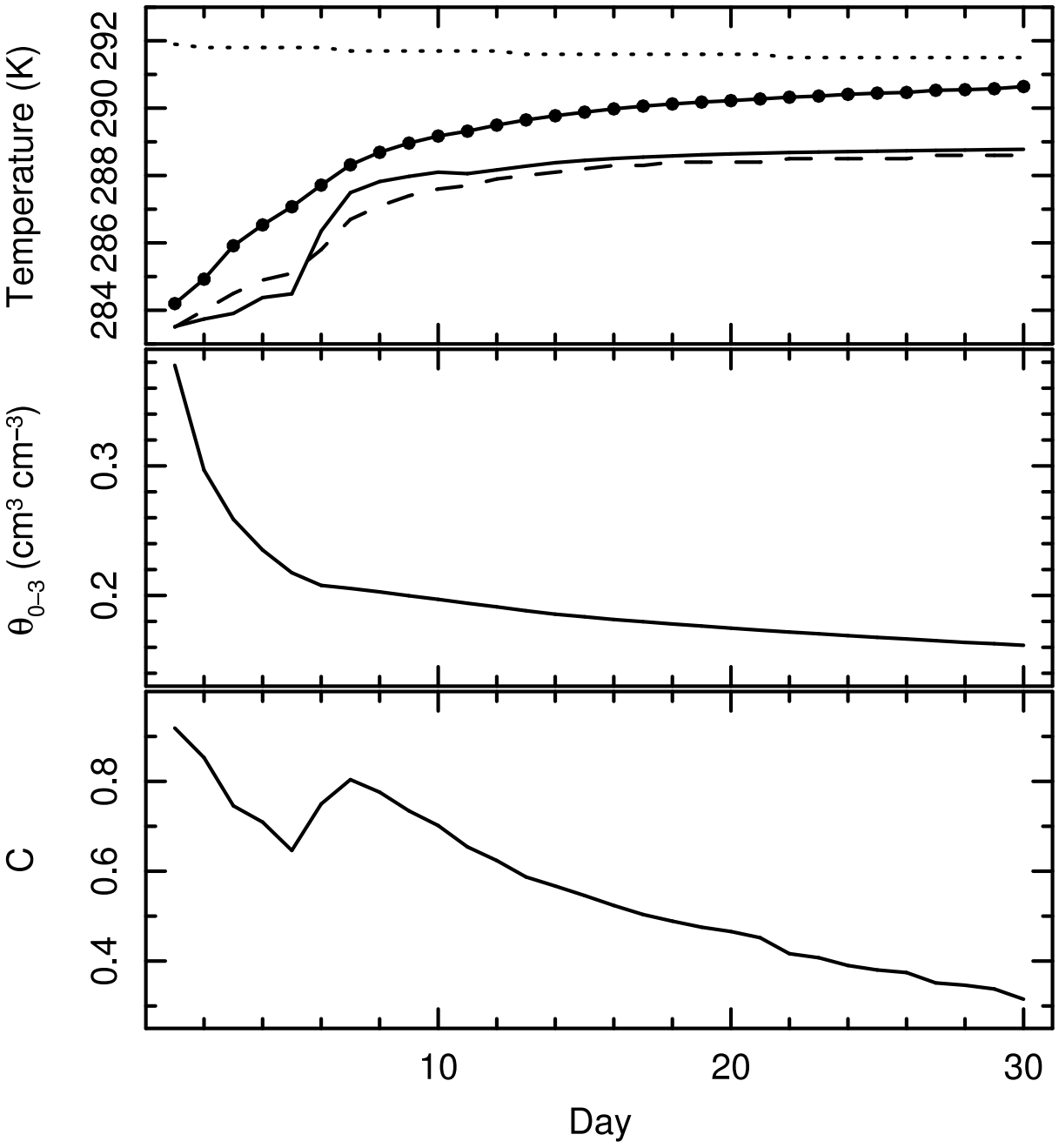

Figure 8: Variation of the 0700 hrs soil temperature (top panel), 0–3 cm volumetric water content (θ_{0-3}; middle panel) and C (bottom panel) over the duration of dry down period, for bare soil. In the top panel, the following temperatures are shown: T_0 (solid line), T_5 (dashed), T_{400} (dotted), and T_{EFF} (solid line with markers).

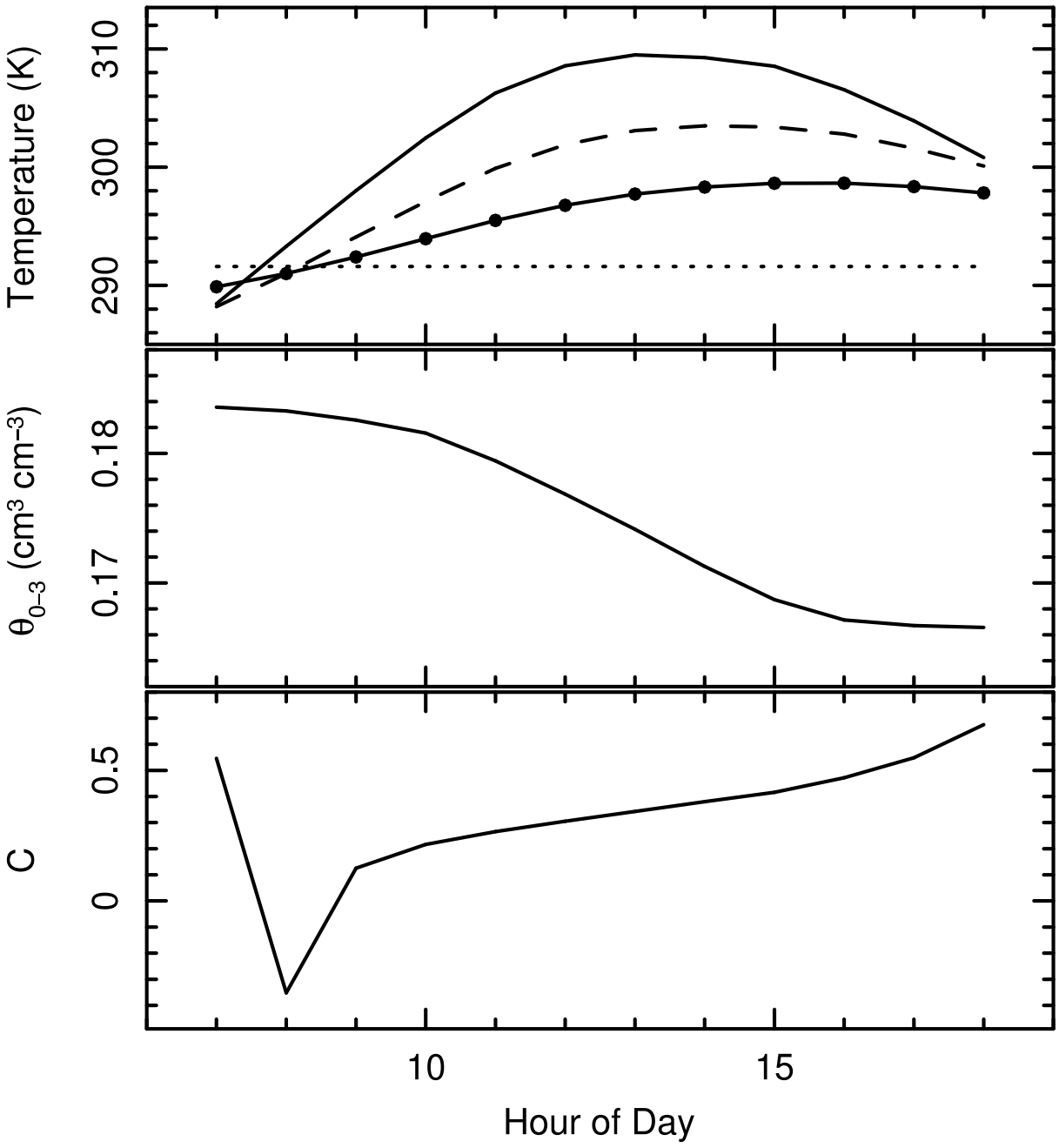

Figure 9: Variation, during day 15, of soil temperature (top panel), 0–3 cm volumetric water content (θ; middle panel) and C (bottom panel), for bare soil. The following temperatures are shown in the top panel: T_0 (solid line), T_5 (dashed), T_{400} (dotted), and T_{EFF} (solid line with markers).

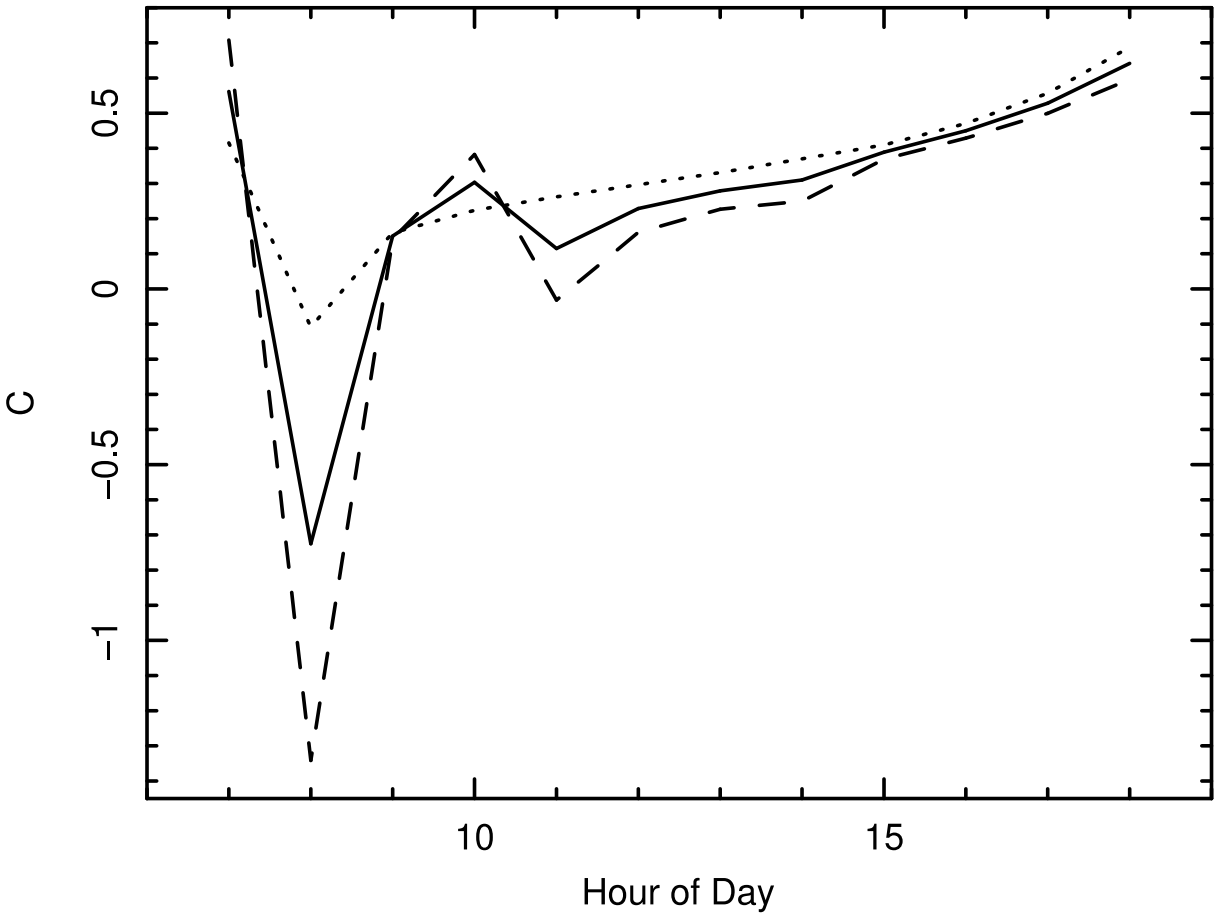

Figure 10: The mean value of C as a function of hour for the entire dry down period (solid line), days 1–15 (dashed) and days 16–30 (dotted).

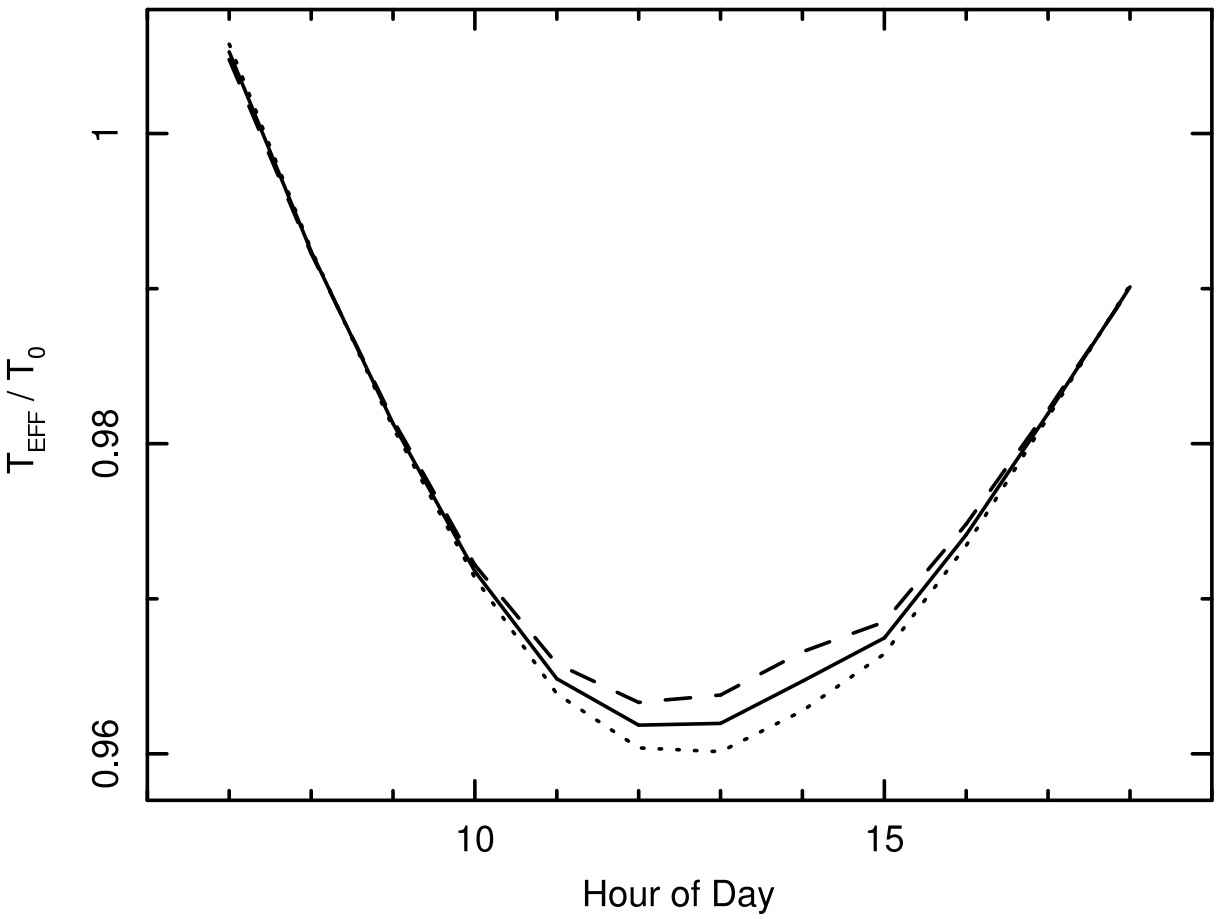

Figure 11: The mean value of the T_{EFF}/T_0 ratio as a function of hour for the entire dry down period (solid line), days 1–15 (dashed) and days 16–30 (dotted).

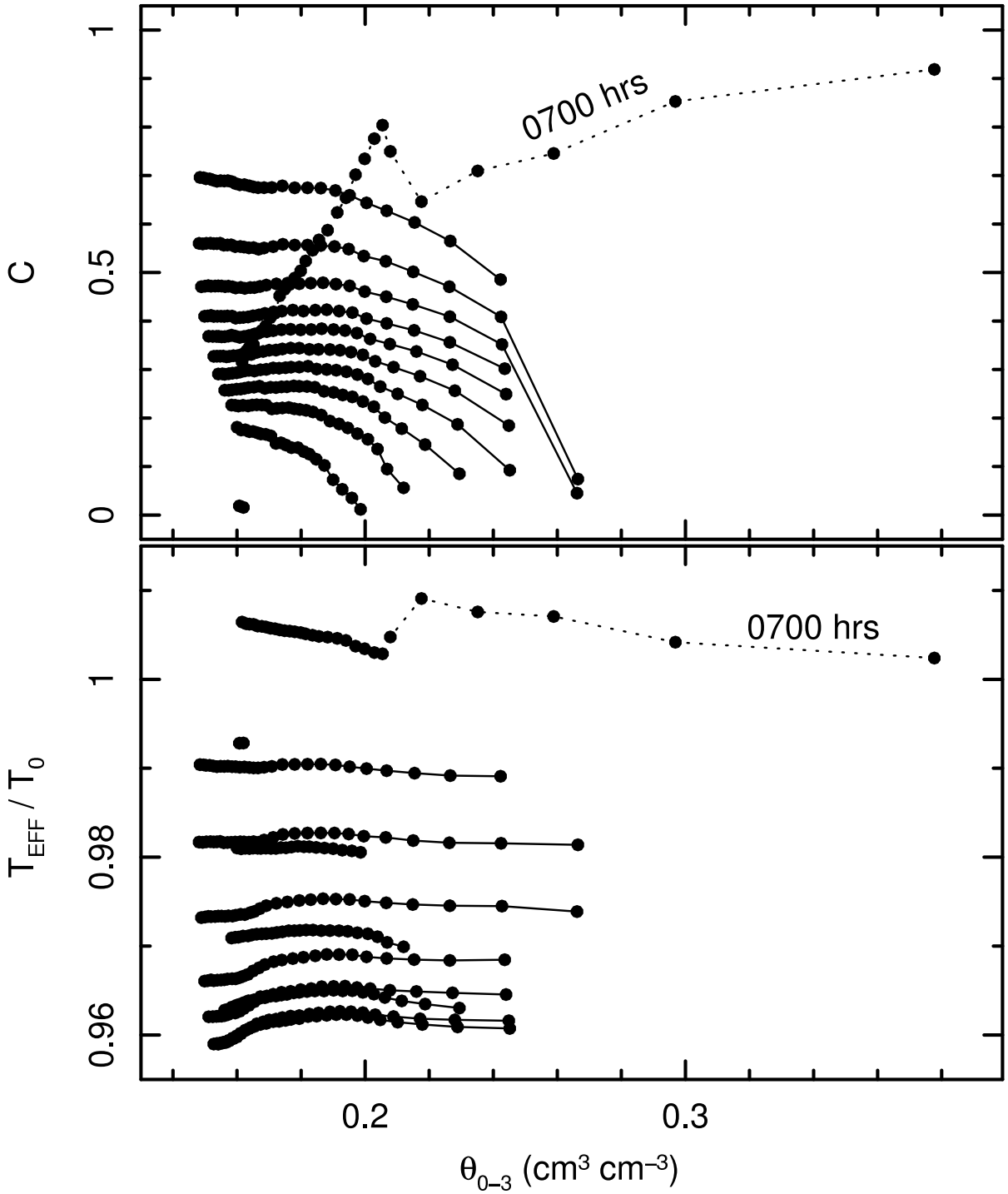

Figure 12: The value of C (top panel) and T_{EFF}/T_0 (bottom panel) as a function of 0–3 cm volumetric water content (θ_{0-3}), for bare soil. Only those profiles for which C was in the range 0–1 are shown. Points corresponding to the same hour are joined by lines. The dotted lines correspond to 0700 hrs.

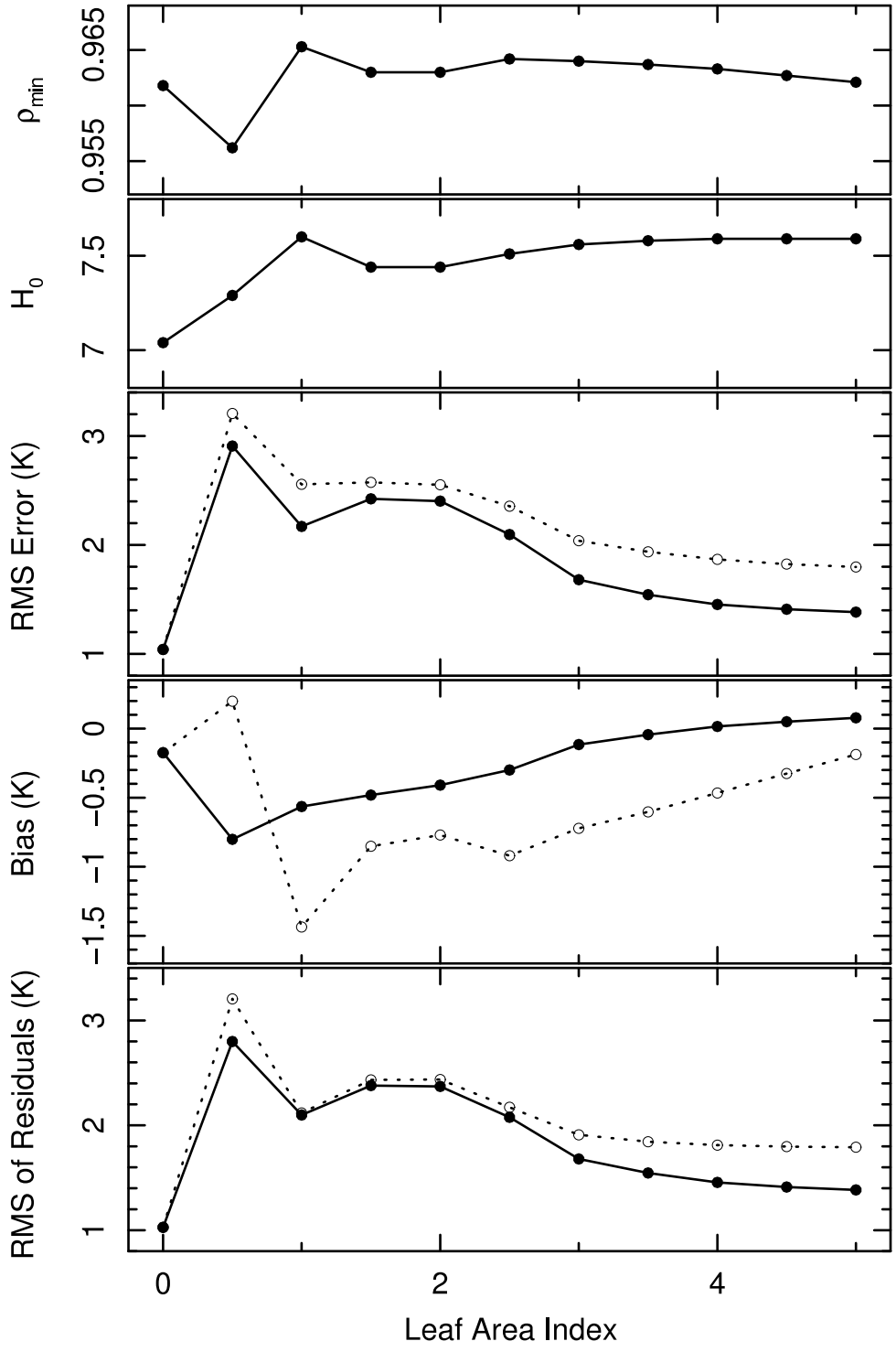

Figure 13: Results from modelling T_{EFF} as a function of T_{TIR} and hour of day, with model parameters $\rho_{\min}$ and H_0 (Model 2; see text for details). The top two panels show the best-fitting parameter values versus leaf area index. The three lower panels, from top to bottom, show the root-mean-square error, bias and standard deviation of the residuals associated with estimating T_{EFF} using the best-fitting parameter values (solid line) and those found for bare soil (dotted).

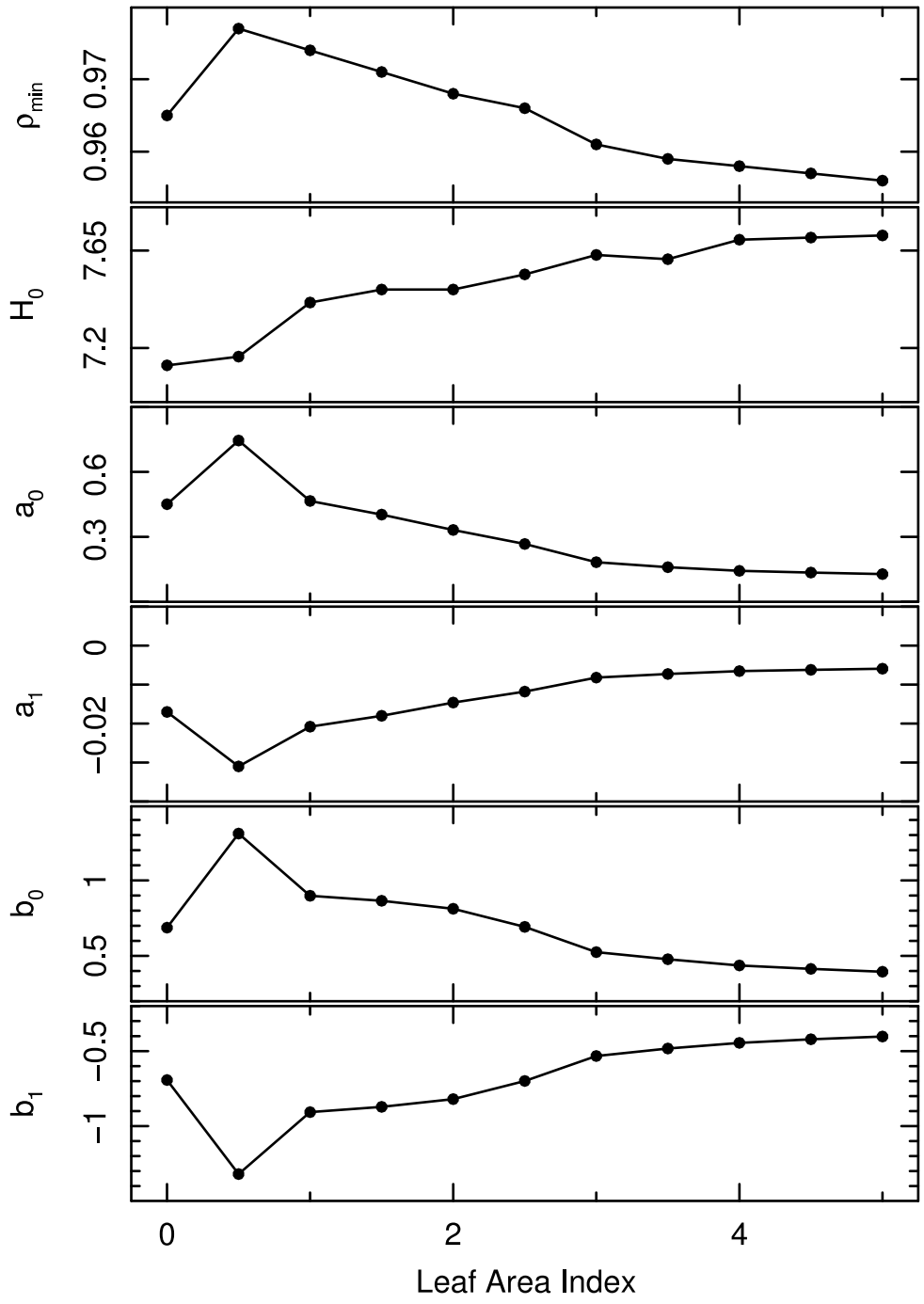

Figure 14: Results from modelling T_{EFF} as a function of T_{TIR}, H and θ_{0-3} (Model 3; see text for details). The model parameters are $\rho_{\min}$, H_0, a_0, a_1, b_0 and b_1. The best-fitting parameter values are plotted versus leaf area index. (See also Fig. 15.)

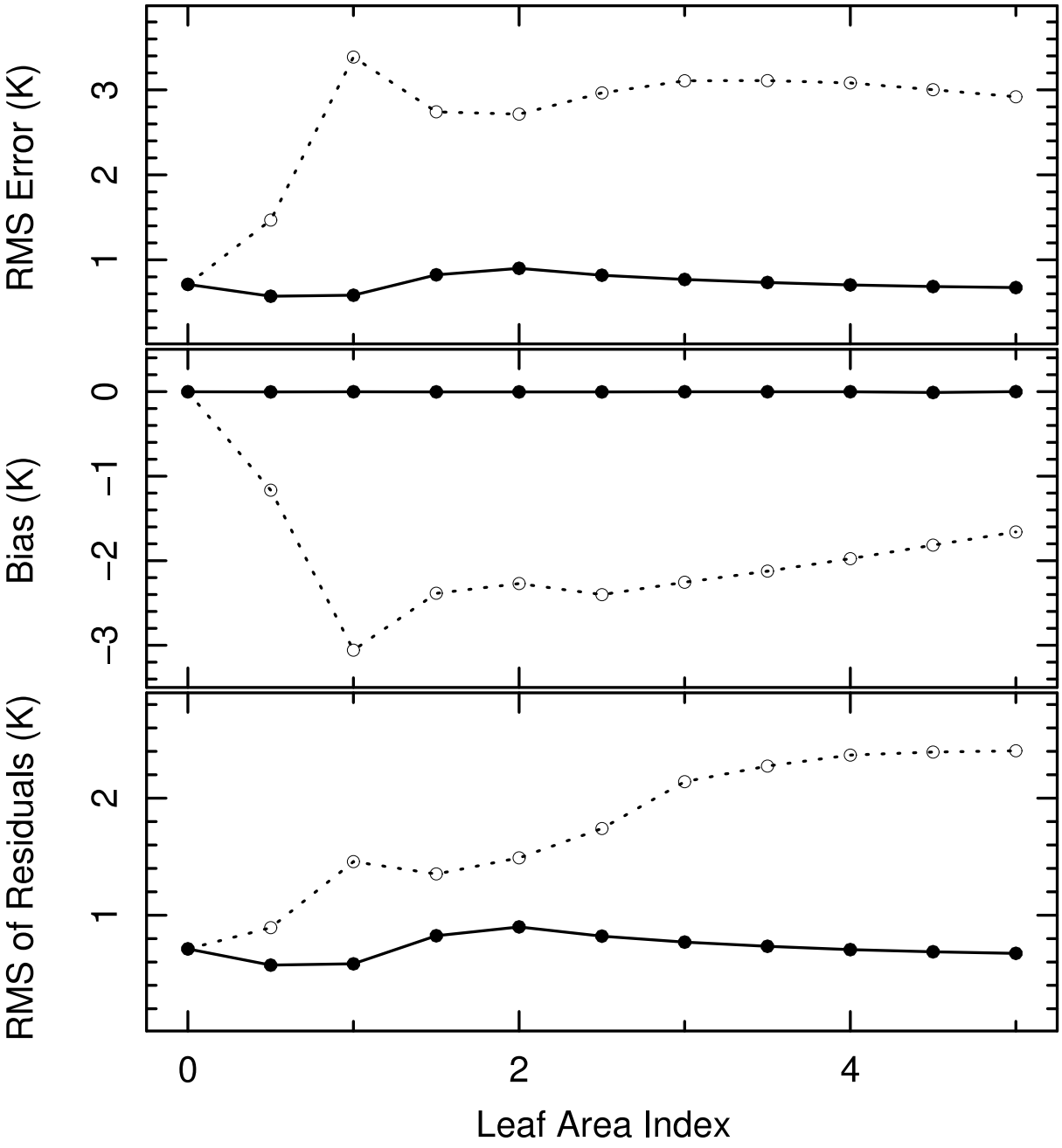

Figure 15: Results from modelling T_{EFF} as a function of T_{TIR}, H and θ_{0-3} (Model 3; see text for details). The three panels, from top to bottom, show the root-mean-square error, bias and standard deviation of the residuals associated with estimating T_{EFF} using the best-fitting parameter values (solid line) and those found for bare soil (dotted).

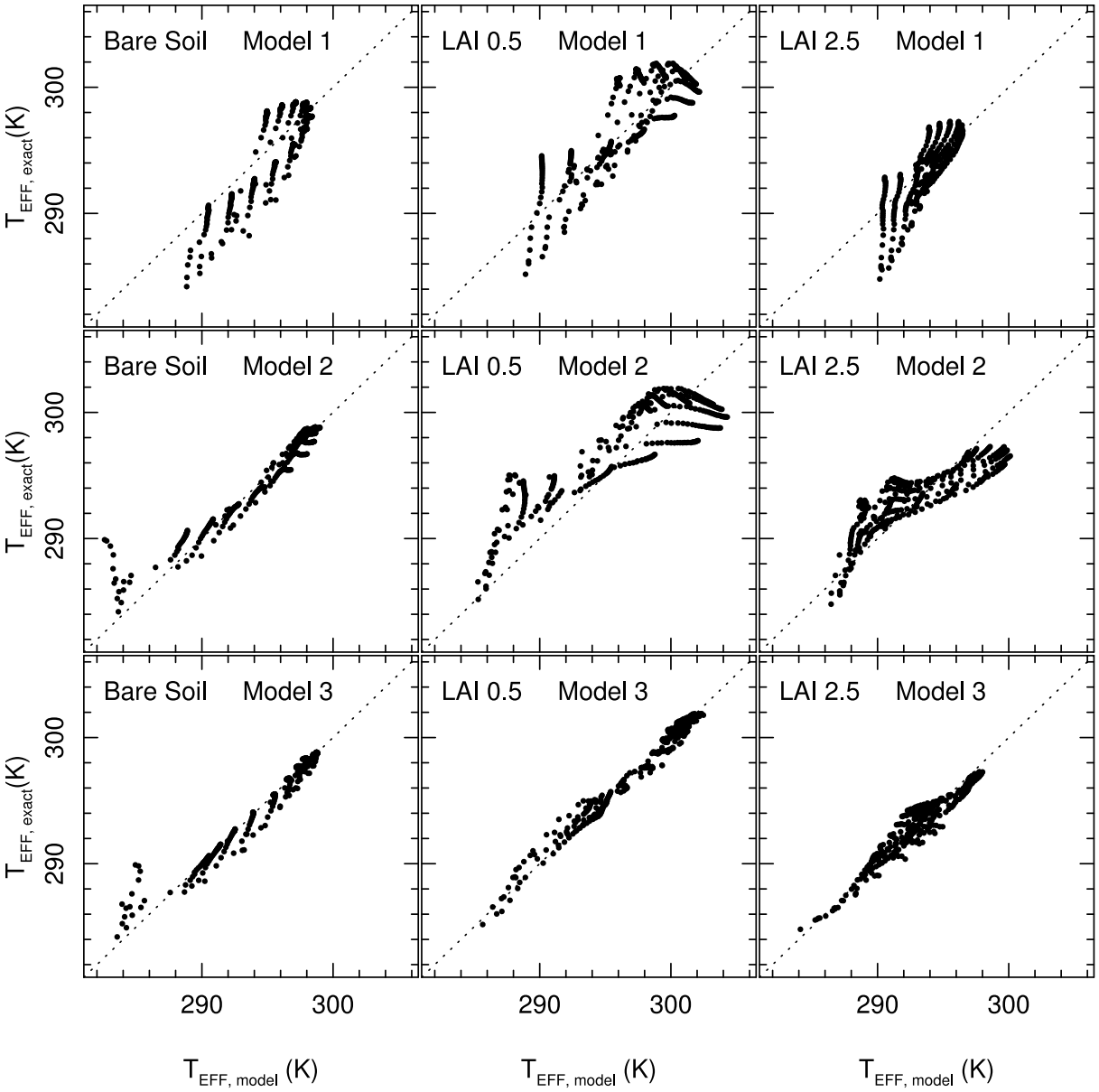

Figure 16: Relationship between the exact value of effective temperature, $T_{\mathrm{EFF,exact}}$ and that estimated, $T_{\mathrm{EFF,model}}$, using Model 1 (C parametrisation; top row), Model 2 (two parameter ratio model; middle row) and Model 3 (six parameter ratio model; bottom row). As well as for bare soil, plots are shown for two representative values of leaf area index (viz., 0.5 and 2.5). The dotted line shows the 1:1 ratio.

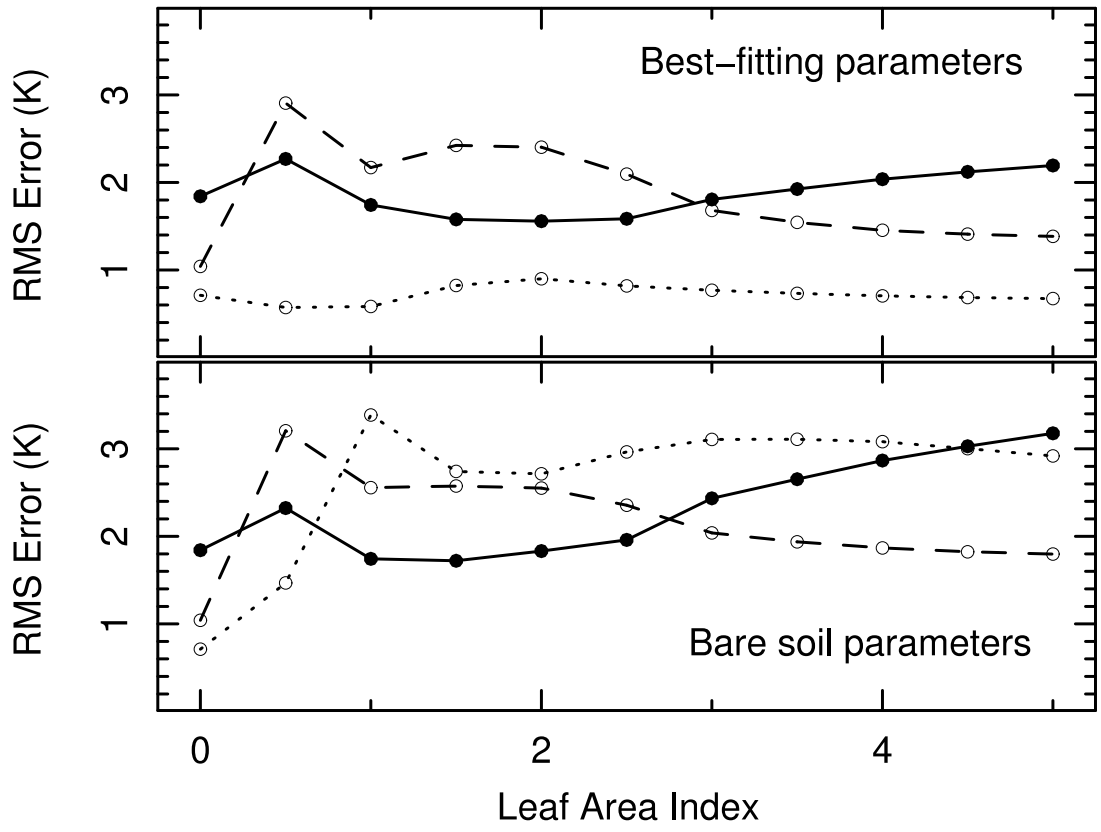

Figure 17: Root-mean-squared error of the residuals associated with estimating $T_{\rm EFF}$ using the best-fitting parameter values (top panel) and those found for bare soil (bottom panel). In each panel the RMS errors for Models 1 (solid line), 2 (dashed) and 3 (dotted) are shown as a function of leaf area index.